Journal of Energy Chemistry 40 (2020) 144–150

Contents lists available at ScienceDirect

Journal of Energy Chemistry

journal homepage: www.elsevier.com/locate/jechem

http://www.journals.elsevier.com/journal-of-energy-chemistry/

Heteroatom substitution-induced asymmetric A–D–A type non-fullerene acceptor for efficient organic solar cells

Chao Li[a,1], Jiali Song[a,1], Yunhao Cai[a], Guangchao Han[b], Wenyu Zheng[b], Yuanping Yi[b], Hwa Sook Ryu[c], Han Young Woo[c], Yanming Sun[a,*]

[a] School of Chemistry, Beihang University, Beijing 100191, China
[b] Beijing National Laboratory for Molecular Science, Key Laboratory of Organic Solids, Institute of Chemistry, Chinese Academy of Sciences, Beijing 100190, China
[c] Department of Chemistry, College of Science, Korea University, Seoul 136-713, Republic of Korea

ARTICLE INFO

Article history:
Received 23 December 2018
Revised 26 February 2019
Accepted 9 March 2019
Available online 13 March 2019

Keywords:
Asymmetric non-fullerene acceptors
Heteroatom substitution
Organic solar cells
Power conversion efficiency

ABSTRACT

Research on asymmetric A–D–A structured non-fullerene acceptors has lagged far behind the development of symmetric counterpart. In this contribution, by simply replacing one sulfur atom in indacenodithiophene unit with a selenium atom, an asymmetric building block SePT and a corresponding asymmetric non-fullerene acceptor SePT-IN have been developed. Asymmetric SePT-IN achieved a high efficiency of 10.20% in organic solar cells when blended with PBT1-C, much higher than that of symmetric TPT-IN counterpart (8.91%). Our results demonstrated an effective heteroatom substitution strategy to develop asymmetric A–D–A structured non-fullerene acceptors.

1. Introduction

In view of the attractive merits of easy tunability in absorption and molecular energy levels through chemical modification, non-fullerene acceptors (NFAs) possessing an acceptor-donor-acceptor (A–D–A) configuration have demonstrated great promise to substitute fullerene acceptors in organic solar cells (OSCs) [1–6], where A and D represent terminal electron-withdrawing unit and central electron-donating unit, respectively. Until now, impressive achievements have been obtained for single-junction OSCs, which are mainly ascribed to the rapid development of A–D–A structured NFAs [7–22]. The chemical structures of the most reported A–D–A structured NFAs are symmetrical. Recently, asymmetric molecular design strategy has been demonstrated as a useful approach to develop high-performance A–D–A structured NFAs [23–28]. However, research on asymmetric A–D–A structured non-fullerene acceptors has still lagged far behind the development of symmetric counterpart [23,26–30].

Five-membered indacedithiophene (IDT) and its derivatives were often utilized as central cores (D) to design asymmetric A–D–A structured NFAs [26,31]. For instance, with symmetric IDT as the central core, Bo and co-workers developed an asymmetric acceptor IDT-OB [26] with asymmetric side chains. When blended with PBDB-T, this IDT-OB showed the power conversion efficiency (PCE) of 10.12%, higher than those of symmetric couterparts (IDT-2O and IDT-2B) bearing symmetric side chains. With the symmetric indacenodithieno[3,2-b]thiophene (IDTT) unit as a central core, Yang and co-workers developed an asymmetric acceptor A2 [31] bearing two different terminal accepting units, which could achieve a promising PCE of 4.52% in OSCs. By changing the thieno[3,2-b]thiophene in central IDTT unit with thieno[2,3-b]thiophene, Yang and co-workers also reported an asymmetric acceptor ITCNTC [32] as an isomer of symmetric acceptor ITCPTC [12]. However, the OSCs based on polymer donor J71 [33] and this asymmetric acceptor ITCNTC blends only gave an inferior PCE of 8.52%, which was much lower than that of the symmetric ITCPTC-based OSCs [34]. Through the rational extension of central IDT backbone conjugation, we had developed a series of high-performing asymmetric A–D–A structured NFAs. For example, with one thiophene or thieno[3,2-b]thiophene fused with the one side of IDT moiety, we had synthesized asymmetric TPTT and TPTTT units as the central cores, along with high-performing asymmetric acceptors TPTT-IC [23] and TPTTT-2F [24], respectively. With one thiophene and one thieno[3,2-b]thiophene simultaneously fused with two sides of IDT moiety, we subsequently designed an asymmetric TTPTTT unit and three TTPTTT-based asymmetric acceptors [25]. All the above results proved that the photovoltaic

* Corresponding author.
E-mail address: sunym@buaa.edu.cn (Y. Sun).
[1] These authors contributed equally to this work.

https://doi.org/10.1016/j.jechem.2019.03.009

performance of some asymmetric NFAs are comparable or even superior to their symmetric counterpart. To further advance and enrich asymmetric A–D–A structured NFAs, a new molecular design strategy to develop asymmetric A–D–A structured NFAs is still highly needed.

In this contribution, we designed a novel asymmetric SePT unit and synthesized an asymmetric acceptor SePT-IN (Fig. 1), in which the sulfur atom in the TPT (or IDT) unit was replaced with the selenium atom. Compared with symmetric acceptor TPT-IN, the asymmetric acceptor SePT-IN exhibited red-shifted absorption, up-shifted HOMO energy level, improved electron mobility and increased intermolecular $\pi-\pi$ stacking interaction. The PBT1-C:SePT-IN blend displayed higher electron mobility, more balanced charge transport and efficient exciton dissociation than PBT1-C:TPT-IN blend. As a result, the optimized device based on SePT-IN delivered a high PCE of 10.20% with a V_{oc} of 0.850 V, a J_{sc} of 16.37 mA cm^{-2} and an FF of 73.3%, much higher than the PCE of 8.91% with a V_{oc} of 0.878 V, a J_{sc} of 13.92 mA cm^{-2} and an FF of 72.9% for the PBT1-C:TPT-IN device. Our results provided another effective molecular design strategy to develop asymmetric A–D–A structured NFAs.

2. Experimental

2.1. Materials synthesis

All reagents and chemicals, which were purchased from commercial sources, were used as received unless other specified. Anhydrous THF was distilled from sodium/benzophenoneketyl prior to use. Unless otherwise specified, all the reactions were performed under the nitrogen atmosphere. Diethyl 2-bromo-5-(thiophen-2-yl)terephthalate and TPT-IN were synthesized according to the literature [23,35]. The number-average molecular weight (M_n) and polydispersity index (PDI) of polymer donor PBT1-C were 34.2 kDa and 1.8, respectively.

2.1.1. Synthesis of diethyl 2-(selenophen-2-yl)-5-(thiophen-2-yl)terephthalate (compound 1)

Under the atmosphere of nitrogen, *n*-BuLi (6.26 mL, 2.5 M in hexane, 15.65 mmol) was added dropwise to a stirring solution of selenophene (2.05 g, 15.65 mmol) in dry THF (100 mL) at −78 °C. After being kept stirring at −78 °C for 1.5 h, tri-n-butyl tin chloride (7.64 g, 23.46 mmol) was then injected into the reaction mixture via a syringe. After the reaction mixture was stirred overnight at room temperature, water was added and the resulting mixture was extracted with dichloromethane. The combined organic layers were dried with anhydrous $MgSO_4$ and the solvent was removed in vacuo to give crude product, which could be used directly for next reaction. To a solution of diethyl 2-bromo-5-(thiophen-2-yl)terephthalate (4.0 g, 10.44 mmol), tributyl(selenophen-2-yl)stannane (6.57 g, 15.65 mmol) and anhydrous toluene (120 mL) was added $Pd(PPh_3)_2Cl_2$ (0.37 g, 0.52 mmol) under nitrogen atmosphere. After the reaction mixture was refluxed overnight, water (100 mL) was added when the reaction mixture was cooled down to room temperature. The mixture was extracted with dichloromethane for three times. The combined organic layers were dried over anhydrous $MgSO_4$ and filtered. The filtrate was concentrated and the residue was purified by column chromatography on silica gel with petroleum ether: dichloromethane (1:1) as an eluent to afford a light yellow solid (4.35 g, 96%). ^{1}H NMR (300 MHz, $CDCl_3$, δ, ppm): 8.09–8.07 (d, 1H), 7.80 (s, 2H), 7.40–7.38 (d, 1H), 7.32–7.30 (t, 1H), 7.23–7.22 (d, 1H), 7.09–7.06 (t, 2H), 4.24–4.19 (q, 4H), 1.17–1.13 (t, 6H). ^{13}C NMR (100 MHz, $CDCl_3$, δ): 167.76, 167.72, 146.39, 140.51, 135.60, 134.02, 133.82, 133.34, 132.36, 131.90, 131.76, 129.71, 129.32, 127.37, 126.97, 126.49, 61.67, 13.82, 13.81. MS (MALDI-TOF) *m/z*: $[M+H]^+$ calcd for $C_{20}H_{18}O_4SSe$, 434.01; found, 434.7.

2.1.2. Synthesis of SePT

To a stirring solution of 1-bromo-4-hexylbenzene (3.34 g, 13.84 mmol) in dry THF (60 mL) at −78 °C was added dropwise *n*-BuLi (5.5 mL, 2.5 M in hexane, 13.84 mmol) under the under the protection of nitrogen. After being kept stirring at −78 °C for 1 h, a solution of compound 1 (1 g, 2.3 mmol) in dry THF (10 mL) was added, then the resulting mixture was warmed to room temperature and stirred overnight. The reaction mixture was poured into water and extracted with dichloromethane for three times. The combined organic phases were dried over with anhydrous $MgSO_4$, filtered and concentrated under reduced pressure. The crude product was directly dissolved in anhydrous dichloromethane (60 mL). Then BF_3 etherate (1 mL) was added and the reaction mixture was stirred for 12 h at room temperature. After evaporation of solvent, the residue was purified by column chromatography on silica gel with petroleum ether: dichloromethane (9:1) as an eluent to give a novel asymmetrical five-membered SePT building block as an off-white solid (1.4 g, 64%). ^{1}H NMR (300 MHz, $CDCl_3$, δ): 7.87–7.85 (d, 1H), 7.41–7.39 (d, 2H), 7.23–7.19 (t, 2H), 7.16–7.13 (m, 8H), 7.05–7.03 (d, 8H), 6.99–6.98 (d, 1H), 2.57–2.52 (t, 8H), 1.59–1.53 (m, 8H), 1.29 (m, 24H), 0.89-0.85 (t, 12H). ^{13}C NMR (100 MHz, $CDCl_3$, δ): 157.53, 155.92, 153.51, 152.86, 144.23, 142.17, 141.98, 141.40, 141.36, 137.54, 135.24, 131.92, 128.34, 127.97, 127.46, 125.75, 123.18, 118.12, 117.15, 63.93, 62.71, 35.65, 31.80, 31.42, 29.22, 22.68, 14.19. MS (MALDI-TOF) *m/z*: $[M+H]^+$ calcd for $C_{64}H_{74}SSe$, 954.47; found, 954.4.

2.1.3. Synthesis of SePT-CHO

Under the protection of nitrogen, *n*-BuLi (2.2 mL, 2.5 M in hexane, 5.57 mmol) was added dropwise to a stirring solution of SePT (1.33 g, 1.40 mmol) in dry THF (60 mL) at −78 °C. After being kept stirring at −78 °C for 1 h, the reaction mixture was stirred at room temperature for another 1 h, which was then cooled to −78 °C again and stirred for 10 min, then anhydrous *N,N*-dimethylformamide (DMF) (1.02 g, 13.94 mmol) was injected into the reaction mixture via a syringe, and the reaction mixture was allowed to warm to room temperature and stirred overnight. The resulting mixture was poured into water, followed by extraction with dichloromethane. The combined organic layers were dried with anhydrous $MgSO_4$ and the solvent was removed in vacuum to give crude product, which was further purified by column chromatography on silica gel with petroleum ether: dichloromethane (1:1) as an eluent to afford a lemon yellow solid (0.63 g, 45%). ^{1}H NMR (300 MHz, $CDCl_3$, δ): 9.82 (s, 1H), 9.69 (s, 1H), 7.88 (s, 1H), 7.65 (s, 1H), 7.58–7.56 (d, 2H), 7.14–7.08 (m, 16H), 2.58–2.55 (t, 8H), 1.58 (m, 8H), 1.30–1.29 (m, 24H), 0.89–0.85 (t, 12H). ^{13}C NMR (100 MHz, $CDCl_3$, δ): 184.02, 182.86, 158.68, 156.97, 155.19, 154.39, 153.53, 151.78, 150.45, 146.36, 142.17, 140.60, 140.49, 138.56, 135.88, 135.18, 132.01, 128.64, 127.66, 119.73, 118.76, 64.25, 62.96, 35.53, 31.69, 31.30, 29.09, 22.58, 14.09. MS (MALDI-TOF) *m/z*: $[M+H]^+$ calcd for $C_{66}H_{74}O_2SSe$, 1010.46; found, 1011.5.

2.1.4. Synthesis of SePT-IN

Under nitrogen atmosphere, SePT-CHO (100 mg, 0.099 mmol), 2-(3-oxo-2,3-dihydro-1H-cyclopenta[b]naphthalen-1-ylidene)malononitrile (97 mg, 0.396 mmol) and chloroform (30 mL) was added to a 50 mL round bottom flask. After the reaction mixture was stirred at room temperature for 10 min, pyridine (0.5 mL) was then added. The reaction mixture was allowed to stir at 65 °C for 12 h. After removal of solvent of reaction mixture, methanol was added and the precipitate was collected by filtration to get crude product, which was further purified by column chromatography on silica gel with petroleum ether:dichloromethane (1:1) as an eluent to afford a black solid (93 mg, 64%). ^{1}H NMR (300 MHz, $CDCl_3$, δ): 9.18–9.16 (d, 2H), 9.02 (s, 1H), 8.95 (s, 1H), 8.35 (s, 2H), 8.04 (m, 4H), 7.93 (s, 1H), 7.73–7.71 (d, 3H), 7.66–7.65 (m, 4H), 7.20–7.12 (m, 16H), 2.62–2.57

(t, 8H), 1.31 (m, 24H), 0.89–0.85 (t, 12H). ^{13}C NMR (100 MHz, $CDCl_3$, δ): 188.67, 188.17, 166.08, 160.44, 160.11, 159.95, 159.59, 158.28, 156.62, 156.01, 144.80, 143.03, 142.47, 142.42, 142.10, 141.53, 140.48, 140.40, 139.75, 138.68, 137.39, 136.26, 135.36, 134.58, 134.44, 132.77, 132.71, 130.66, 130.19, 129.95, 129.68, 128.85, 127.74, 126.98, 124.60, 124.26, 123.55, 120.80, 119.88, 115.19, 115.01, 68.01, 67.83, 64.18, 63.02, 35.61, 31.74, 31.36, 29.72, 29.12, 22.61, 14.13. MS (MALDI-TOF) *m/z*: $[M + H]^+$ calcd for $C_{98}H_{86}N_4O_2SSe$, 1462.56; found, 1463.4.

2.2. Materials characterization

^{1}H NMR and ^{13}C NMR spectra were recorded on a Bruker Avance 300 spectrometer with deuterated chloroform ($CDCl_3$) and trimethylsilane (TMS) as the solvent and internal reference, respectively. UV-visible absorption spectra were performed by a Hitachi (model U-3010) UV–vis spectrophotometer. Mass spectra were recorded on Bruker Daltonics Biflex III MALDI-TOF Analyzer in the MALDI mode. Cyclic voltammetry (CV) measurements were conducted under nitrogen atmosphere at a scan rate of 100 mV s^{-1} using a Zahner IM6e Electrochemical workstation. A platinum plate coated with sample film, a saturated Ag/Ag^+ electrode and platinum wire were used as a working electrode, a reference electrode and a counter electrode, respectively. Ferrocene/ferrocenium (Fc/Fc^+) and 0.1 M tetra-n-butylammonium hexafluorophosphate (Bu_4NPF_6) in anhydrous acetonitrile solution were employed as an internal standard and a supporting electrolyte, respectively. The onset oxidation potential of ferrocene external standard was measured to be 0.43 eV in our group. Therefore, the LUMO and HOMO energy level could be calculated according to the equations: LUMO = – (E_{red}^{onset} + 4.37) eV and HOMO = –(E_{ox}^{onset} + 4.37) eV, where E_{red}^{onset} and E_{ox}^{onset} were the onset reduction potential and onset oxidation potential relative to Ag/Ag^+, respectively. Atomic force microscopy (AFM) measurements were carried out utilizing a Dimension Icon AFM (Bruker) in the tapping mode. GIWAXS measurements were performed at PLS-II 9A U-SAXS beamline of the Pohang Accelerator Laboratory in Korea.

2.3. Organic solar cells fabrication and characterization

Organic solar cells with an inverted device architecture of ITO/ZnO/photoactive layer/MoO_3/Ag were fabricated. The ITO-coated glass substrates were cleaned successively by ultrasonic treatment in detergent deionized water, acetone and isopropyl alcohol for 20 min, respectively. After drying for one night, ZnO precursor solution was spin-coated at 4000 rpm, and the ZnO layer was generated at 200 °C for 15 min in ambient atmosphere. The active layers were spin-coated from a solution of PBT1-C:NFA with weight ratio of 1:1 in chloroform. Solution with 0.25 v% DIO was stirred overnight prior to cast. The active layers were allowed to heat at 100 °C for 10 min in a N_2-filled glovebox. The MoO_3 were deposited by sequential thermal evaporation of 3 nm followed by 90 nm of Ag. A Keithley 2400 Source Measure Unit was used to measure the current density–voltage (*J–V*) characteristics. The currents were determined under 100 mW/cm^2 simulated 1.5 Global (AM 1.5G) solar simulator (Enli Technology Co., Ltd, SS-F5-3A). A standard silicon (Si) solar cell (SRC-2020, Enli Technology Co., Ltd) was used to calibrate the light intensity. EQE spectra were performed by utilizing the solar-cell spectral-response measurement system (QE-R, Enlitech).

2.4. Space-charge limited current measurement

The charge transport properties were evaluated by space charge limited current (SCLC) measurement. The electron-only devices and hole-only devices were fabricated with a structure of ITO/ZnO/PBT1-C:NFA/ZrAcac/Al and ITO/PEDOT:PSS/PBT1-C:NFA/MoO_3/Ag, respectively. The *J–V* curves of devices were fitted by using the Mott–Gurney equation: $J = 9\varepsilon_0\varepsilon_r\mu V^2/8L^3$, in which *J* was the current density, ε_0 was the permittivity of free space, ε_r was the permittivity of the active layer, μ was the hole/electron mobility, *V* was the internal voltage of the device ($V = V_{appl} - V_{bi}$), where V_{app} was the applied voltage, V_{bi} was the offset voltage (V_{bi} is 0 V here), and *L* was the film thickness of the active layer. The electron/hole mobility could be measured from the slope of the $J^{0.5}$–*V* curve.

3. Results and discussion

The synthesis of SePT-IN was presented in Scheme 1. Firstly, diethyl 2-bromo-5-(thiophen-2-yl)terephthalate was reacted with tributyl(selenophen-2-yl)stannane through the Stille coupling reaction to afford compound 1. Subsequently, compound 1 was treated with (4-hexylphenyl)lithium to give two benzyl alcohols, which was subjected to Friedel–Crafts cyclization to lead to a novel asymmetric SePT. Afterwards, this asymmetric SePT was reacted with n-butyllithium followed by addition of anhydrous DMF to afford SePT-CHO. Finally, the SePT-CHO was reacted with 2-(3-oxo-2,3-dihydro-1H-cyclopenta[b]naphthalen-1-ylidene)malononitrile via the Knoevenagel condensation reaction to provide asymmetric SePT-IN. This SePT-IN could be readily soluble in commonly used organic solvents, such as chloroform, chlorobenzene and dichlorobenzene. The symmetric TPT-IN was also synthesized for comparison according to the literature [35]. All the newly synthesized compounds were fully characterized using ^{1}H NMR, ^{13}C NMR, and MS (MALDI-TOF) and their structural characterizations could be found in the Supporting Information.

Density functional theory (DFT) calculations were carried out to investigate the electronic structure properties of symmetric TPT-IN and asymmetric SePT. The computational details could be found in the Supporting Information. The calculated results were shown in Fig. S1 and Table S1. The energy gap between LUMO+1 and LUMO was less than 0.4 eV for both compounds, suggesting that the LUMO+1 could accept electrons from the LUMO of the polymer donor [36]. For both NFAs, the LUMO and LUMO+1 were delocalized over the whole molecular backbone, whereas the HOMO was relatively localized on the central TPT/SePT unit. Compared with TPT-IN, the calculated LUMO energy level was slightly downshifted while the HOMO energy level was slightly upshifted, resulting in a smaller band gap in SePT-IN.

The normalized absorption spectra of the symmetric TPT-IN and asymmetric SePT-IN were presented in Fig. 2, and the corresponding optical data were listed in Table 1. The asymmetric SePT-IN showed a maximum absorption peak at 698 nm in solution, which has a 13 nm red shift relative to the symmetric TPT-IN. From solution to solid state, both two NFAs showed considerable red-shifted absorption spectrum and broader absorption profile than their respective solution counterpart. Specifically, the maximum absorption peaks of TPT-IN and SePT-IN were red-shifted from 685 to 727 nm and 698 to 741 nm, respectively. The redshifted absorption of SePT-IN than TPT-IN was resulted from the stronger electron-donating ability and more quinodal structure of selenophene relative to thiophene. The thin film absorption onsets of TPT-IN and SePT-IN were centered at 786 and 803 nm, which corresponded to optical bandgaps of 1.58 and 1.54 eV, respectively.

The electrochemical properties of the symmetric TPT-IN and asymmetric SePT-IN were investigated by cyclic voltammetry (CV) measurements. As depicted in Fig. 2(b), the onset oxidation/reduction potentials of TPT-IN and SePT-IN were 1.43/−0.40 and 1.40/−0.37 V vs. Ag/Ag^+, respectively. The HOMO/LUMO energy levels of TPT-IN and SePT-IN were then determined to

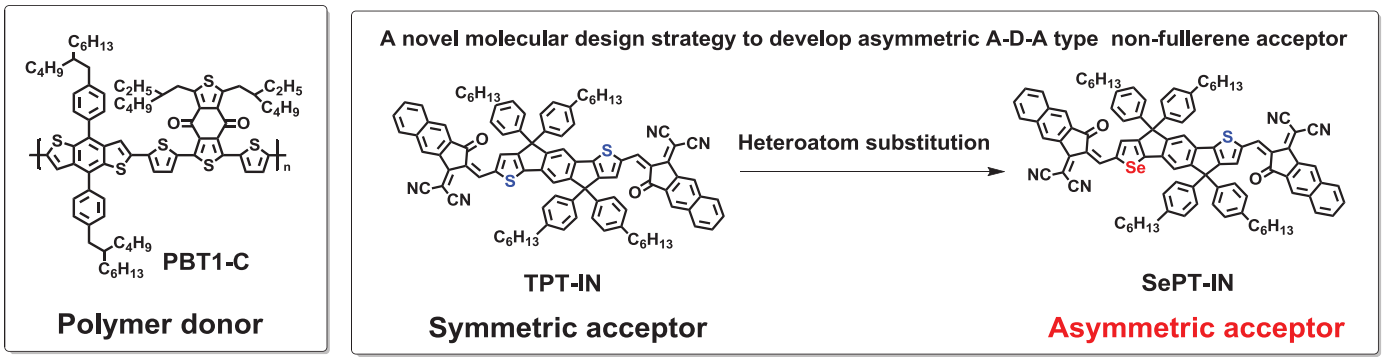

Fig. 1. Chemical structures of PBT1-C, TPT-IN and SePT-IN.

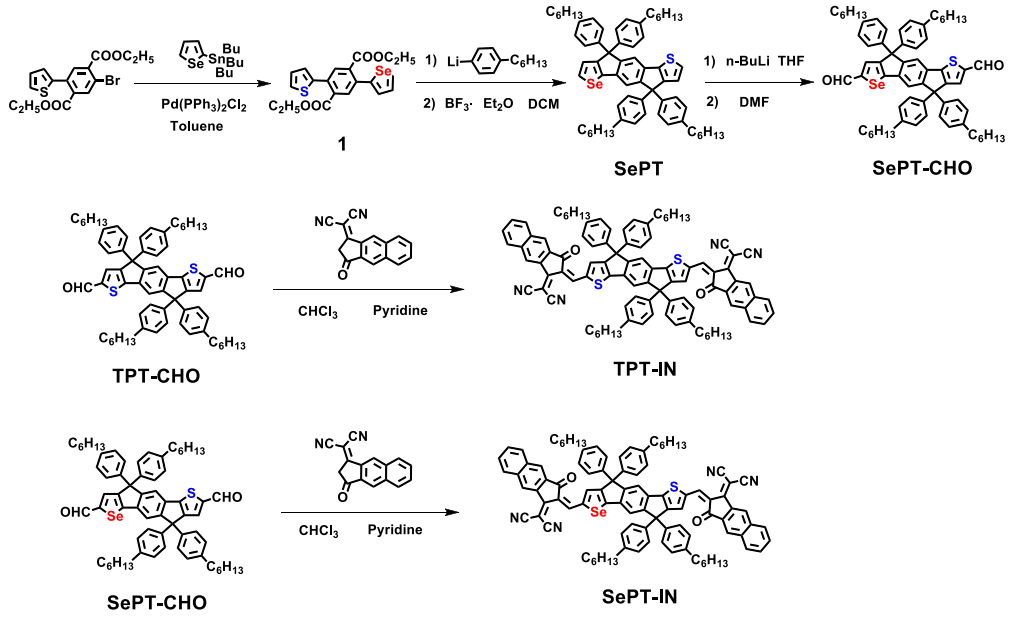

Scheme 1. Synthetic routes of symmetric TPT-2F and asymmetric SePT-IN.

Table 1. Optical and electrochemical properties of TPT-IN and SePT-IN.

NFA	λ_{max}[a] (nm)	λ_{max}[b] (nm)	λ_{onset}[b] (nm)	E_g^{opt}[c] (eV)	E_{ox} (V)	HOMO (eV)	E_{red} (V)	LUMO (eV)
TPT-IN	685	727	786	1.58	1.43	−5.80	−0.40	−3.97
SePT-IN	698	741	803	1.54	1.40	−5.77	−0.37	−4.00

[a] In chloroform solution.
[b] In a thin film drop cast from the chloroform solution.
[c] Calculated from the empirical formula: $E_g^{opt} = 1240/\lambda_{onset}$.

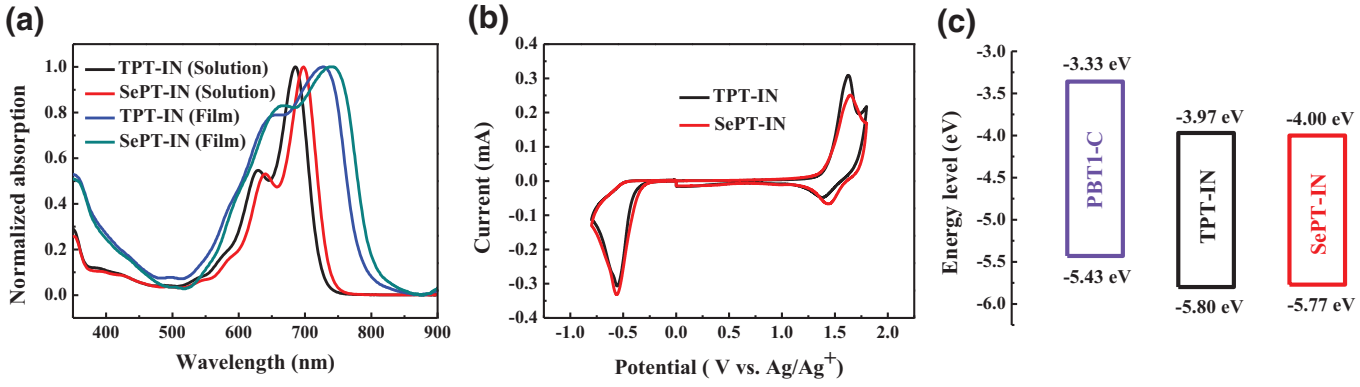

Fig. 2. (a) Normalized absorption spectra of symmetric TPT-IN and asymmetric SePT-IN in chloroform solution and in thin film. (b) Cyclic voltammograms of symmetric TPT-IN and asymmetric SePT-IN. (c) Energy level diagram of PBT1-C, symmetric TPT-IN and asymmetric SePT-IN.

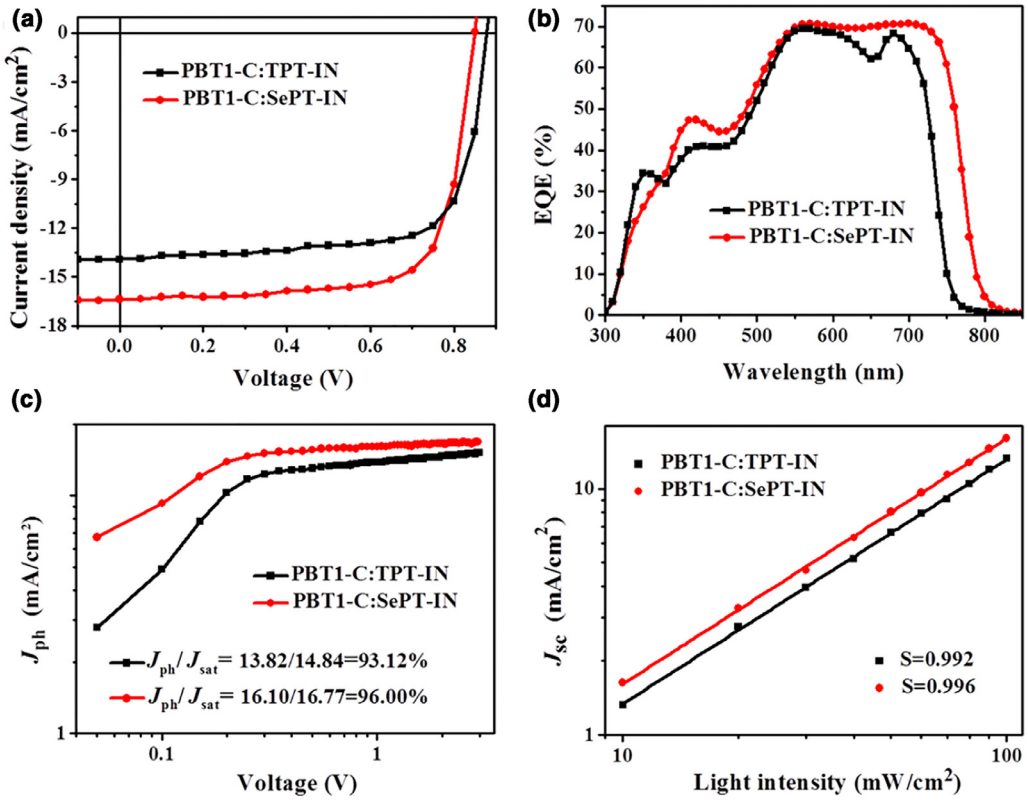

Fig. 3. (a) *J*–*V* curves, (b) EQE spectra, (c) J_{ph} vs. V_{eff} plot and (d) light intensity dependence of J_{sc} of the optimized devices based on the PBT1-C:NFA blend.

Table 2. Photovoltaic parameters of optimized PBT1-C:NFA device.

NFA	V_{oc} (V)	J_{sc} (mA cm^{-2})	$J_{sc,cal}$ (mA cm^{-2})	FF (%)	PCE[a] (%)
TPT-IN	0.878 (0.876±0.003)	13.92 (14.09±0.12)	13.45	72.9 (71.38±1.11)	8.91 (8.75±0.18)
SePT-IN	0.850 (0.847±0.001)	16.37 (16.01±0.14)	15.81	73.3 (73.18±0.28)	10.20 (10.00±0.16)

[a] Average values with standard deviations were obtained from 20 devices.

be −5.80/−3.97 and −5.77/−4.00 eV, respectively. These results demonstrated that replacing the thiophene in TPT unit with selenophene upshifted HOMO energy level as a result of stronger electron-donating ability and reduced aromaticity of selenophene than that of thiophene [37], and interestingly downshifted LUMO energy level at the meanwhile.

The photovoltaic properties of the two NFAs were investigated by fabricating the OSC devices with an inverted device structure of ITO/ZnO/PBT1-C:NFA/MoO_3/Ag, where PBT1-C was employed as donor material [38]. The optimized OSC devices were obtained by employing chloroform as the processing solvent with donor/acceptor (D/A) weight ratio of 1:1 and 1,8-diiodooctane (DIO) content of 0.25% (Figs. S3 and S4, Tables S2 and S3). The current density–voltage (*J*–*V*) curves and photovoltaic parameters of the optimized OSC devices were presented in Fig. 3 and Table 2, respectively. The optimized device based on asymmetric SePT-IN afforded a decent PCE of 10.20% with a V_{oc} of 0.850 V, a J_{sc} of 16.37 mA cm^{-2} and an FF of 73.3%. In contrast, the optimized device based on symmetric TPT-IN showed a slightly lower PCE of 8.91% with a V_{oc} of 0.878 V, a J_{sc} of 13.92 mA cm^{-2} and an FF of 72.9%. The higher PCE in optimized PBT1-C:SePT-IN device was mainly ascribed to its higher J_{sc} and slightly higher FF, while the relatively lower V_{oc} in optimized PBT1-C:SePT-IN device was in agreement with the downshifted LUMO energy level of SePT-IN relative to TPT-IN.

The external quantum efficiency (EQE) curves of the optimized devices were shown in Fig. 3(b). The SePT-IN based device exhibited a broad photoresponse in the region of 300–800 nm, while the TPT-IN based device only displayed a broad photoresponse ranging from 300 to 750 nm. Besides, the maximum EQE value of SePT-IN based device was slightly higher than that of TPT-IN based device. As a result, a high integrated J_{sc} of 15.81 mA cm^{-2} was obtained for the PBT1-C:SePT-IN device, which was higher than that of the PBT1-C:TPT-IN device (13.45 mA cm^{-2}). The result demonstrated that incident photon-to-current efficiency was higher in SePT-IN based device. These integrated J_{sc} values were consistent with the J_{sc} values extracted from *J*–*V* curves within 5% mismatch.

The charge transport properties of the two NFA neat films and corresponding blend films were evaluated by space charge limited current (SCLC) measurement. As presented in Fig. S5 and Table S4, the electron mobilities of the neat TPT-IN and SePT-IN films were measured to be 4.74×10^{-4} and 7.07×10^{-4} cm^2 V^{-1} s^{-1}, respectively. These results indicated that substituting one thiophene in symmetric TPT-IN with one selenophene increased the electron mobility. In the blend films, the hole/electron mobilities of PBT1-C:TPT-IN and PBT1-C:SePT-IN blend films were determined to be $13.8 \times 10^{-4}/3.96 \times 10^{-4}$ and $12.6 \times 10^{-4}/6.35 \times 10^{-4}$ cm^2 V^{-1} s^{-1}, which corresponded to μ_h/μ_e ratios of 3.48 and 1.98, respectively. Obviously, the PBT1-C:SePT-IN blend film displayed a higher electron mobility and a more balanced charge carrier mobility than PBT1-C:TPT-IN blend film, which agreed with the higher J_{sc} and slightly higher FF observed in PBT1-C:SePT-IN device.

To investigate the exciton dissociation and charge collection properties, the photocurrent density (J_{ph}) vs. the effective volt-

age (V_{eff}) was measured. As shown in Fig. 3(c), the saturated J_{ph} (J_{sat}) values could be obtained for both devices at a V_{eff} greater than 2 V, indicating that all the photogenerated excitons were dissociated into free charge carriers and collected by the electrodes. The J_{sat} value of the PBT1-C:SePT-IN device was determined to be 16.77 mA cm^{-2}, which was higher than the J_{sat} value of 14.84 mA cm^{-2} for the PBT1-C:TPT-IN device, demonstrating that the PBT1-C:SePT-IN device exhibited enhanced charge generation and thus increased J_{sc} [39]. Under the short-circuit condition, the J_{ph}/J_{sat} ratios of the PBT1-C:TPT-IN and PBT1-C:SePT-IN devices were estimated to be 93.12% and 96.00%, respectively, indicating that the PBT1-C:SePT-IN device had more efficient exciton dissociation and charge collection efficiency than that of PBT1-C:TPT-IN device [40].

To investigate the charge recombination behavior, the dependence of the photocurrent (J_{ph}) on different light intensities (P_{light}) was measured. The relationship between J_{sc} and P could be described by the formula of $J_{sc} \propto P_{light}^{S}$, in which the exponential factor S represented the extent of the bimolecular recombination. As presented in Fig. 3(d), the S values of PBT1-C:TPT-IN and PBT1-C:SePT-IN devices were measured to be 0.992 and 0.996, respectively, suggesting that both two blend devices had negligible bimolecular charge recombination.

The surface morphology of optimized blend films was investigated by atomic force microscopy (AFM). As depicted in Fig. 4, in the AFM height images, both blend films exhibited smooth and uniform surfaces with root-mean-square (RMS) roughness of 1.35 nm for PBT1-C:TPT-IN blend film and 1.53 nm for PBT1-C:SePT-IN blend film. In the AFM phase images, a fibril network morphology occurred in both blend films, which is helpful for efficient charge transport in the OSC devices [30].

To explore the molecular orientation and packing behaviors in neat and blend films, two dimensional grazing incidence wide angle X-ray scattering (2D GIWAXS) measurements were performed. The 2D GIWAXS patterns and corresponding line-cuts profiles were shown in Fig. 5. Both NFA neat films had a face-on dominant orientation relative to the substrate, as supported by a strong (100) scattering peak in the in-plane (IP) direction and a strong (010) scattering peak in the out-of-plane (OOP) direction. In Fig. 5(b), both neat films showed similarly a π-π stacking peak at ~1.76 Å^{-1}, which corresponded to a π-π stacking distance of 3.57 Å. However, as can be clearly seen in Fig. 5(a), the (010) π–π diffraction intensity in the SePT-IN neat film was stronger than that of TPT-IN neat film, suggesting that replacing thiophene in NFAs with selenophene increases the intermolecular π–π stacking interactions, which may facilitate efficient charge transport in a vertical direction. In both of their blend films, the predominant face-on orientation maintained and the resulting π–π stacking distance was slightly increased to 3.63–3.67 Å for both blends compared to the pristine films. However, PBT1-C:TPT-IN showed a hump-shaped (100) peak together with the complicated fine scattering patterns, indicating the increased edge-on oriented crystallites compared to pristine films. The fine structures may be originated from several differently structured crystallites, which are probably due to the poor miscibility of PBT1-C and symmetrical TPT-IN relative to the PBT1-C:SePT-IN blend.

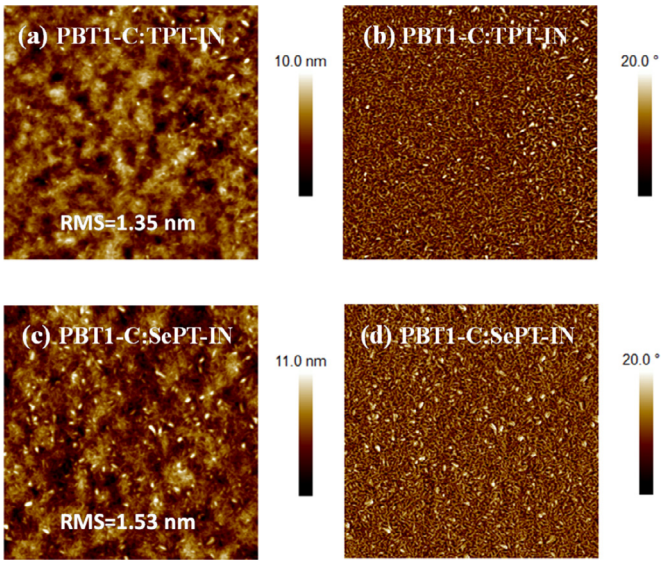

Fig. 4. AFM height images (a, c) and phase images (b, d) of the optimized blend films. The scan size of the AFM images is 2 × 2 μm^2.

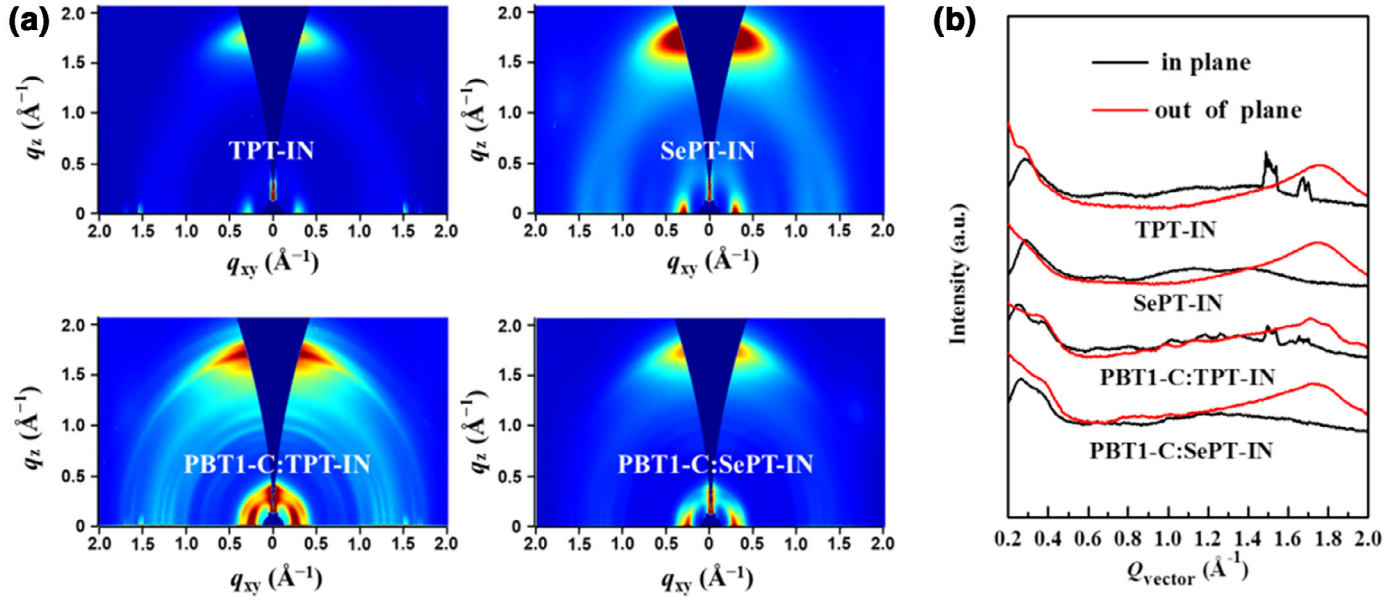

Fig. 5. (a) 2D GIWAXS patterns of TPT-IN, SePT-IN and their corresponding blend films; (b) in-plane (black lines) and out-of-plane (red lines) line-cut profiles of 2D GIWAXS results.

4. Conclusions

In summary, a new asymmetric selenium-substituted central core SePT was developed by simply replacing one thiophene in indacenodithiophene (TPT) building block with one selenophene. The central core SePT was coupled with 2-(3-oxo-2,3-dihydro-1H-cyclopenta[b]naphthalen-1-ylidene)malononitrile to furnish an asymmetric A–D–A structured non-fullerene acceptor SePT-IN. The replacement of one thiophene in the TPT unit with one selenophene endowed SePT-IN with an asymmetric structure, a red-shifted absorption, upshifted HOMO energy level, an enhanced electron mobility and an increased intermolecular π-π stacking interaction relative to symmetric acceptor TPT-IN. When this asymmetric acceptor SePT-IN blended with PBT1-C, the optimized device based on SePT-IN delivered a decent PCE of 10.20%, which was higher than that (8.91%) of TPT-IN-based devices. We proposed an effective heteroatom substitution strategy toward the synthesis of high-performance asymmetric A–D–A structured non-fullerene acceptors.

Acknowledgments

This work was financially supported by the National Natural Science Foundation of China (NSFC) (Nos. 21674007 and 21734001). HYW acknowledges the financial support from National Research Foundation (NRF) of Korea (2012M3A6A7055540 and 2015M1A2A2057506).

Supplementary material

Supplementary material associated with this article can be found, in the online version, at doi:10.1016/j.jechem.2019.03.009.

References

[1] D. He, F. Zhao, L. Jiang, C. Wang, J. Mater. Chem. A 6 (2018) 8839–8854.
[2] F. Shen, J. Xu, X. Li, C. Zhan, J. Mater. Chem. A 6 (2018) 15433–15455.
[3] J. Hou, O. Inganäs, R.H. Friend, F. Gao, Nat. Mater. 17 (2018) 119.
[4] C. Yan, S. Barlow, Z. Wang, H. Yan, A.K.Y. Jen, S.R. Marder, X. Zhan, Nat. Rev. Mater. 3 (2018) 18003.
[5] G. Zhang, J. Zhao, P.C.Y. Chow, K. Jiang, J. Zhang, Z. Zhu, J. Zhang, F. Huang, H. Yan, Chem. Rev. 118 (2018) 3447–3507.
[6] Z.-Q. Jiang, T.-T. Wang, F.-P. Wu, J.-D. Lin, L.-S. Liao, J. Mater. Chem. A 6 (2018) 17256–17287.
[7] Y. Lin, J. Wang, Z.-G. Zhang, H. Bai, Y. Li, D. Zhu, X. Zhan, Adv. Mater. 27 (2015) 1170–1174.
[8] S. Li, L. Ye, W. Zhao, X. Liu, J. Zhu, H. Ade, J. Hou, Adv. Mater. 29 (2017) 1704051.
[9] W. Zhao, S. Li, H. Yao, S. Zhang, Y. Zhang, B. Yang, J. Hou, J. Am. Chem. Soc. 139 (2017) 7148–7151.
[10] Y. Lin, F. Zhao, Q. He, L. Huo, Y. Wu, T.C. Parker, W. Ma, Y. Sun, C. Wang, D. Zhu, A.J. Heeger, S.R. Marder, X. Zhan, J. Am. Chem. Soc. 138 (2016) 4955–4961.
[11] S. Li, L. Ye, W. Zhao, S. Zhang, S. Mukherjee, H. Ade, J. Hou, Adv. Mater. 28 (2016) 9423–9429.
[12] D. Xie, T. Liu, W. Gao, C. Zhong, L. Huo, Z. Luo, K. Wu, W. Xiong, F. Liu, Y. Sun, C. Yang, Sol. RRL 1 (2017) 1700044.
[13] B. Kan, H. Feng, H. Yao, M. Chang, X. Wan, C. Li, J. Hou, Y. Chen, Sci. China Chem. 61 (2018) 1307–1313.
[14] X. Liu, B. Xie, C. Duan, Z. Wang, B. Fan, K. Zhang, B. Lin, F.J.M. Colberts, W. Ma, R.A.J. Janssen, F. Huang, Y. Cao, J. Mater. Chem. A 6 (2018) 395–403.
[15] W. Su, Q. Fan, X. Guo, J. Chen, Y. Wang, X. Wang, P. Dai, C. Ye, X. Bao, W. Ma, M. Zhang, Y. Li, J. Mater. Chem. A 6 (2018) 7988–7996.
[16] Y. Yang, Z.-G. Zhang, H. Bin, S. Chen, L. Gao, L. Xue, C. Yang, Y. Li, J. Am. Chem. Soc. 138 (2016) 15011–15018.
[17] Z. Fei, F.D. Eisner, X. Jiao, M. Azzouzi, J.A. Röhr, Y. Han, M. Shahid, A.S.R. Chesman, C.D. Easton, C.R. McNeill, T.D. Anthopoulos, J. Nelson, M. Heeney, Adv. Mater. 30 (2018) 1705209.
[18] X. Shi, L. Zuo, S.B. Jo, K. Gao, F. Lin, F. Liu, A.K.Y. Jen, Chem. Mater. 29 (2017) 8369–8376.
[19] H. Wu, H. Fan, S. Xu, C. Zhang, S. Chen, C. Yang, D. Chen, F. Liu, X. Zhu, Sol. RRL 1 (2017) 1700165.
[20] Y. Li, X. Liu, F.-P. Wu, Y. Zhou, Z.-Q. Jiang, B. Song, Y. Xia, Z.-G. Zhang, F. Gao, O. Inganäs, Y. Li, L.-S. Liao, J. Mater. Chem. A 4 (2016) 5890–5897.
[21] B. Kan, H. Feng, X. Wan, F. Liu, X. Ke, Y. Wang, Y. Wang, H. Zhang, C. Li, J. Hou, Y. Chen, J. Am. Chem. Soc. 139 (2017) 4929–4934.
[22] J. Yuan, Y. Zhang, L. Zhou, G. Zhang, H.-L. Yip, T.-K. Lau, X. Lu, C. Zhu, H. Peng, P.A. Johnson, M. Leclerc, Y. Cao, J. Ulanski, Y. Li, Y. Zou, Joule (2019), doi:10.1016/j.joule.2019.01.004.
[23] C. Li, Y. Xie, B. Fan, G. Han, Y. Yi, Y. Sun, J. Mater. Chem. C 6 (2018) 4873–4877.
[24] J. Song, C. Li, L. Ye, C. Koh, Y. Cai, D. Wei, H.Y. Woo, Y. Sun, J. Mater. Chem. A 6 (2018) 18847–18852.
[25] C. Li, J. Song, L. Ye, C. Koh, K. Weng, H. Fu, Y. Cai, Y. Xie, D. Wei, H.Y. Woo, Y. Sun, Sol. RRL 3 (2019) 1800246.
[26] S. Feng, C.e. Zhang, Y. Liu, Z. Bi, Z. Zhang, X. Xu, W. Ma, Z. Bo, Adv. Mater. 29 (2017) 1703527.
[27] W. Gao, M. Zhang, T. Liu, R. Ming, Q. An, K. Wu, D. Xie, Z. Luo, C. Zhong, F. Liu, F. Zhang, H. Yan, C. Yang, Adv. Mater. 30 (2018) 1800052.
[28] W. Zhai, A. Tang, B. Xiao, X. Wang, F. Chen, E. Zhou, Sci. Bull. 63 (2018) 845–852.
[29] W. Gao, Q. An, C. Zhong, Z. Luo, R. Ming, M. Zhang, Y. Zou, F. Liu, F. Zhang, C. Yang, Chem. Sci. 9 (2018) 8142–8149.
[30] C. Li, T. Xia, J. Song, H. Fu, H.S. Ryu, K. Weng, L. Ye, H.Y. Woo, Y. Sun, J. Mater. Chem. A 7 (2019) 1435–1441.
[31] Y. Zhao, Z. Luo, G. Li, J. Luo, Z.-G. Zhang, Y. Li, C. Yang, Chem. Commun. 54 (2018) 9801–9804.
[32] Z. Luo, G. Li, K. Wu, Z.-G. Zhang, X. Chen, B. Qiu, L. Xue, Y. Li, C. Yang, Org. Electron. 62 (2018) 82–88.
[33] H. Bin, L. Gao, Z.-G. Zhang, Y. Yang, Y. Zhang, C. Zhang, S. Chen, L. Xue, C. Yang, M. Xiao, Y. Li, Nat. Commun. 7 (2016) 13651.
[34] Z. Luo, H. Bin, T. Liu, Z.-G. Zhang, Y. Yang, C. Zhong, B. Qiu, G. Li, W. Gao, D. Xie, K. Wu, Y. Sun, F. Liu, Y. Li, C. Yang, Adv. Mater. 30 (2018) 1706124.
[35] R. Li, G. Liu, M. Xiao, X. Yang, X. Liu, Z. Wang, L. Ying, F. Huang, Y. Cao, J. Mater. Chem. A 5 (2017) 23926–23936.
[36] A. Kuzmich, D. Padula, H. Ma, A. Troisi, Energy Environ. Sci. 10 (2017) 395–401.
[37] Z. Fei, Y. Han, E. Gann, T. Hodsden, A.S.R. Chesman, C.R. McNeill, T.D. Anthopoulos, M. Heeney, J. Am. Chem. Soc. 139 (2017) 8552–8561.
[38] T. Liu, L. Huo, S. Chandrabose, K. Chen, G. Han, F. Qi, X. Meng, D. Xie, W. Ma, Y. Yi, J.M. Hodgkiss, F. Liu, J. Wang, C. Yang, Y. Sun, Adv. Mater. 30 (2018) 1707353.
[39] W. Wang, C. Yan, T.-K. Lau, J. Wang, K. Liu, Y. Fan, X. Lu, X. Zhan, Adv. Mater. 29 (2017) 1701308.
[40] S. Dai, T. Li, W. Wang, Y. Xiao, T.-K. Lau, Z. Li, K. Liu, X. Lu, X. Zhan, Adv. Mater. 30 (2018) 1706571.